

LETTER TO THE EDITOR

First JWST observations of a gravitational lens

Mass model of new multiple images with near-infrared observations of SMACS J0723.3–7327

G. B. Caminha¹*, S. H. Suyu^{1,2,3}, A. Mercurio⁴, G. Brammer^{5,6}, P. Bergamini^{7,8}, A. Acebron⁷, and E. Vanzella⁸

¹ Max-Planck-Institut für Astrophysik, Karl-Schwarzschild-Str. 1, D-85748 Garching, Germany

² Technische Universität München, Physik-Department, James-Frank Str. 1, 85748 Garching, Germany

³ Academia Sinica Institute of Astronomy and Astrophysics (ASIAA), 11F of ASMA, No.1, Section 4, Roosevelt Road, Taipei 10617, Taiwan

⁴ INAF - Osservatorio Astronomico di Capodimonte, Via Moiariello 16, I-80131 Napoli, Italy

⁵ Cosmic Dawn Center (DAWN), Denmark

⁶ Niels Bohr Institute, University of Copenhagen, Jagtvej 128, DK-2200 Copenhagen N, Denmark

⁷ Dipartimento di Fisica, Università degli Studi di Milano, Via Celoria 16, I-20133 Milano, Italy

⁸ INAF - Osservatorio Astronomico di Bologna, via Gobetti 93/3, 40129 Bologna, Italy

July 18, 2022

ABSTRACT

We present our lens mass model of SMACS J0723.3–7327, the first strong gravitational lens observed by the *James Webb Space Telescope* (*JWST*). We use data from the *Hubble Space Telescope* and Multi Unit Spectroscopic Explorer (MUSE) to build our “pre-*JWST*” lens model, and refine it with newly available *JWST* near-infrared imaging in our *JWST* model. To reproduce the positions of all multiple lensed images with good accuracy, the adopted mass parameterization consists of one cluster-scale component, accounting mainly for the dark matter distribution, the galaxy cluster members and an external shear component. The pre-*JWST* model has, as constraints, 19 multiple images from six background sources, of which four have secure spectroscopic redshift measurements from this work. The *JWST* model has more than twice the number of constraints, 27 additional multiple images from another ten lensed sources. Both models can reproduce very well the multiple image positions with a δ_{rms} of 0′:39 and 0′:51, for the pre-*JWST* and *JWST* models, respectively. The total mass estimates within a radius of 128 kpc (roughly the Einstein radius) are $7.9^{+0.3}_{-0.2} \times 10^{13} M_{\odot}$ and $8.6^{+0.2}_{-0.2} \times 10^{13} M_{\odot}$, for the pre-*JWST* and *JWST* models, respectively. We predict with our mass models the redshifts of the newly detected *JWST* sources, which are crucial information especially for systems without spectroscopic measurements for further studies and follow-up observations. Interestingly, one family detected with *JWST* is found to be at a very high redshift, $z > 7.5$ (68% confidence level) and with one image having lensing magnification of $|\mu| = 9.8^{+0.9}_{-1.1}$, making it an interesting case for future studies. The lens models, including magnification maps and redshifts estimated from the model are made publicly available, along with the full spectroscopic redshift catalogue from MUSE.

Key words. Galaxies: clusters: individual: SMACS J0723.3–7327 – Gravitational lensing: strong – cosmology: observations – dark matter

1. Introduction

Galaxy clusters are the most massive structures in the Universe, and are therefore powerful cosmic telescopes for observing faint and distant sources via the gravitational lensing effect (e.g., Atek et al. 2015). When a background source galaxy lies behind a galaxy cluster, the light rays that we see from the source are deflected by the gravitational potential of the foreground galaxy cluster, i.e., the source is gravitationally lensed by the cluster. In the regime of strong lensing, we see multiple magnified and distorted images of the background source. The lensing magnifications produced by galaxy cluster can reach factors of $\sim 100 - 1000$, allowing us to detect the faintest sources that would be otherwise impossible (see e.g. Caminha et al. 2016b; Vanzella et al. 2020, 2021). The positions and morphologies of

the multiple lensed images also allow us to probe the distribution of matter, particularly dark matter, in the galaxy cluster, which is crucial for understanding the nature of dark matter (e.g., Bradač et al. 2006; Clowe et al. 2006). Furthermore, an individual galaxy cluster often lenses several background sources into several corresponding “families” of multiple images that straddle at different locations around the galaxy cluster. Families of multiple images formed by sources of different redshifts provide measurements of angular diameter distance ratios between the cluster and sources, allowing us to probe the geometry of the Universe (Jullo et al. 2010; Acebron et al. 2017; Caminha et al. 2016a, 2022). In cases where a background source is time varying, such as a quasar or supernova, the time delay(s) between the multiple images provide measurements of the “time-delay distance” and the Hubble constant that sets the expansion rate of the Universe (Refsdal 1964; Suyu et al. 2010; Kelly et al. 2015; Grillo et al. 2018, 2020). Strong lensing galaxy clusters

* e-mail address: caminha@mpa-garching.mpg.de. The electronica material is available in this link: https://wwwmpa.mpa-garching.mpg.de/~caminha/SMACS0723_Caminha/

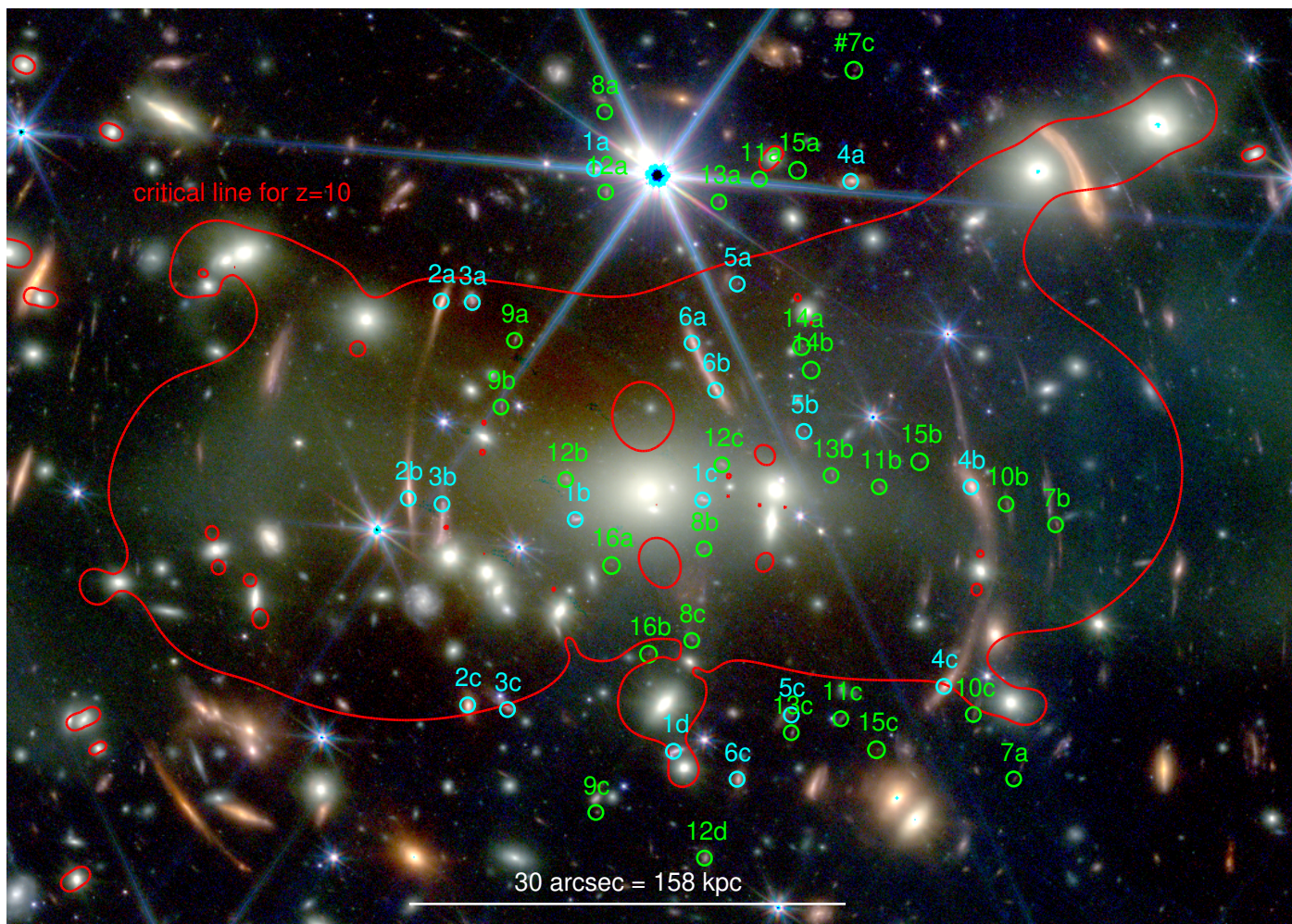


Fig. 1. The galaxy cluster SMACS J0723. Colour composed image using *JWST*/NIRCam imaging with the filters F090W, F150W in blue; F200W, F277W in green; and F356W and F444W in red. Cyan circles show the positions of multiple images identified in the pre-*JWST* lens model and the green circles are the newly identified multiple images with *JWST*. The red line is the critical line for a source at redshift $z = 10$.

are therefore excellent laboratories for astrophysical and cosmological studies.

The *James Webb Space Telescope* (*JWST*, Rigby et al. 2022) operating in the infrared will provide unprecedented observations of high-redshift galaxies, both in terms of sensitivity and angular resolution. Studying these distant galaxies is crucial for understanding how the first galaxies form and evolve into the structures that we see today. These first galaxies are inherently faint, and the combination of *JWST* and galaxy cluster is therefore the best way to detect and study these faintest galaxies. As part of the Early Release Observations (ERO), *JWST* publicly released the observations of its first cosmic targets, including the galaxy cluster SMACS J0723.3–7327 (hereafter SMACS J0723, discovered by Ebeling et al. 2001 and Repp & Ebeling 2018). In this letter, we demonstrate the power of strong gravitational lensing and *JWST* to unveil and study faint distant galaxies. In particular, we identify new sources in the *JWST* images that were previously undetected in the Hubble Space Telescope (*HST*) imaging, more than doubling the number of families of multiple images. Even though these new families of images do not yet have spectroscopic redshifts, we demonstrate the utility of our cluster lens mass model to constrain the redshifts of these new source galaxies, including one at $z > 6$.

Our paper is organized as follows. In Section 2, we present the pre-*JWST* archival data of the galaxy cluster SMACS J0723.

The *JWST* observations used in this work are presented in Section 3. In Section 4, we present our lens models based on archival data only (pre-*JWST*), the updated version including new multiple images identified with *JWST*, and a comparison to other models in the literature. Finally, we summarize in Section 5.

2. Pre-*JWST* archival data

In this section, we describe the data used in this work, consisting of *HST* photometry and MUSE spectroscopy for building the pre-*JWST* lens model.

2.1. *HST*

Observations from *HST* of SMACS J0723 were obtained under the treasury programme Reionization Lensing Cluster Survey (RELICS, Coe et al. 2019). Imagings were obtained in the filters F435W, F606W and F814W using the Advanced Camera for Surveys, and F105W, F125W, F140W and F160W using the Wide Field Camera 3. All reduced images and catalogues are publicly available in the Mikulski Archive for Space Telescope¹. The imaging and color information were used to identify multi-

¹ <https://archive.stsci.edu/prepds/relics/>

Table 1. Multiple image list.

ID	RA	Dec	z	$ \mu $
1a	110.8302653775	-73.4484703860	$1.84^{+0.09}_{-0.08}$	$4.3^{+0.4}_{-0.5}$
1b	110.8315839500	-73.4551704511	"	$3.8^{+0.7}_{-0.6}$
1c	110.8230386287	-73.4548011166	"	$1.5^{+0.4}_{-0.3}$
1d	110.8250107058	-73.4595997391	"	$11.6^{+3.4}_{-2.1}$
2a	110.8405365164	-73.4509957549	1.4503	$9.8^{+1.4}_{-1.3}$
2b	110.8427758496	-73.4547637941	1.4503	$23.3^{+5.1}_{-4.2}$
2c	110.8388129336	-73.4587087766	1.4503	$6.8^{+0.9}_{-0.8}$
3a	110.8384630963	-73.4510225059	1.3782	$9.2^{+1.3}_{-1.2}$
3b	110.8405113048	-73.4548709934	1.3782	103^{+153}_{-47}
3c	110.8361429009	-73.4587973008	1.3782	$6.1^{+0.7}_{-0.7}$
4a	110.8130876147	-73.4487156625	$2.20^{+0.09}_{-0.08}$	$5.8^{+0.7}_{-0.7}$
4b	110.8050431160	-73.4545561509	"	$14.2^{+2.6}_{-2.5}$
4c	110.8068620127	-73.4583655711	"	$9.6^{+1.3}_{-1.3}$
5a	110.8207007748	-73.4506760494	1.3825	$9.1^{+1.3}_{-1.3}$
5b	110.8162335526	-73.4534926339	1.3825	$12.9^{+1.8}_{-1.9}$
5c	110.8171039789	-73.4589088990	1.3825	$5.2^{+0.6}_{-0.7}$
6a	110.8237341404	-73.4518040104	1.4254	$30.0^{+7.8}_{-6.4}$
6b	110.8221590678	-73.4527025651	1.4254	$43.4^{+7.4}_{-5.6}$
6c	110.8207468206	-73.4601341978	1.4254	$3.8^{+0.4}_{-0.4}$
7a†	110.8021918024	-73.4601348271	> 7.5	$6.0^{+0.8}_{-0.9}$
7b†	110.7993733038	-73.4552793576	"	$9.8^{+1.1}_{-1.1}$
#7c†	110.8128699466	-73.4465944181	—	$4.5^{+0.5}_{-0.5}$
8a†	110.8295676112	-73.4473859288	$1.88^{+0.07}_{-0.06}$	$3.4^{+0.3}_{-0.3}$
8b†	110.8229423834	-73.4557325725	"	$10.9^{+1.7}_{-1.6}$
8c†	110.8237732631	-73.4574832535	"	$21.4^{+4.7}_{-3.9}$
9a†	110.8356387152	-73.4517465412	$1.67^{+0.04}_{-0.03}$	$45.4^{+15.3}_{-10.8}$
9b†	110.8365547868	-73.4530182644	"	$18.1^{+2.1}_{-2.1}$
9c†	110.8302221440	-73.4607653275	"	$3.9^{+0.4}_{-0.4}$
10b†	110.8026934208	-73.4548842598	$3.10^{+0.28}_{-0.22}$	$13.7^{+2.4}_{-2.5}$
10c†	110.8048945912	-73.4589021013	"	$9.2^{+1.2}_{-1.2}$
11a†	110.8192030143	-73.4486729318	$1.87^{+0.07}_{-0.06}$	$5.4^{+0.6}_{-0.6}$
11b†	110.8111947441	-73.4545527988	"	$6.8^{+1.0}_{-1.0}$
11c†	110.8137839019	-73.4589815364	"	$6.4^{+0.8}_{-0.8}$
12a†	110.8295177750	-73.4489165365	$2.65^{+0.26}_{-0.20}$	$6.1^{+0.7}_{-0.8}$
12b†	110.8322177002	-73.4544051992	"	$3.9^{+0.8}_{-0.7}$
12c†	110.8217443301	-73.4541282431	"	$6.4^{+1.3}_{-1.2}$
12d†	110.8229393279	-73.4616409371	"	$3.7^{+0.3}_{-0.3}$
13a†	110.8219242869	-73.4491076284	$1.68^{+0.06}_{-0.05}$	$5.3^{+0.6}_{-0.6}$
13b†	110.8144209400	-73.4543348989	"	$4.5^{+0.8}_{-0.8}$
13c†	110.8171117496	-73.4592453685	"	$5.5^{+0.6}_{-0.6}$
14a†	110.8163947858	-73.4518737634	$1.46^{+0.58}_{-0.21}$	$45.9^{+40.6}_{-26.9}$
14b†	110.8157525822	-73.4523225418	"	$42.1^{+41.2}_{-27.6}$
15a†	110.8166488501	-73.4485063451	$2.29^{+0.12}_{-0.10}$	$5.2^{+0.6}_{-0.6}$
15b†	110.8084789438	-73.4540734888	"	$7.9^{+1.0}_{-1.2}$
15c†	110.8113960548	-73.4595739183	"	$5.6^{+0.6}_{-0.6}$
16a†	110.8291533467	-73.4560496998	$2.05^{+0.41}_{-0.28}$	$10.1^{+2.4}_{-1.9}$
16b†	110.8266763430	-73.4577453680	"	$18.6^{+3.4}_{-3.8}$

Notes. IDs, coordinates (RA and Dec), redshifts (z) and magnifications ($|\mu|$) of all multiple images. Exact redshift values are spectroscopic confirmations, and values with 68% confidence level uncertainties are obtained from the *JWST* lens model. Lensing magnifications are also from the *JWST* model. IDs marked with † are objects detected with the release of *JWST* data. Image #7c is only a candidate (indicated with the #) and not used in the model, although its morphology and colors strongly indicate it is a correct identification in family 7.

ple images and cluster members with no spectroscopic information. More details are presented in Section 4.1.

2.2. VLT/MUSE

MUSE data of this field are available in the ESO Science Archive Facility². The field was observed in the programme ID 0102.A-0718 (P.I.: A. Edge) under fair conditions of seeing $\approx 0.7''$ and moon illumination of 68%, and with an exposure time of 2910 seconds on target. We processed the raw-data following all steps in the standard reduction pipeline (version 2.8.3, [Weilbacher et al. 2020](#)). To improve the sky-subtraction, we used the autocalibration mode and also applied the Zurich Atmosphere Purge (ZAP, [Soto et al. 2016](#)) on the data. The final data-cube has 1 arcmin² field of view and covers the wavelength range of 4750Å to 9350Å.

We extracted the 1D spectra from all *HST* detected sources to measure their redshifts. In a second step, we performed a blind search to detect faint emission lines with no clear photometric counterpart. We refer the reader to our previous works ([Caminha et al. 2019, 2017b,a](#)) for more details on this procedure. Our final redshift catalogue contains 78 secure and precise redshifts measurements and is presented in Table A.1, and also in the electronic version of this manuscript.

3. JWST Early Release Observations

SMACS J0723 is the first gravitational lens observed by *JWST*. It was one of the targets of the ERO carried out during the telescope commissioning. The observations obtained photometric data from Near Infrared Camera (NIRCam; e.g., [Rieke et al. 2005](#)) and Mid-Infrared Instrument (MIRI; [Rieke et al. 2015, Bouchet et al. 2015](#)), and spectroscopy from Near Infrared Spectrograph (NIRSpec; [Jakobsen et al. 2022](#)) and Near Infrared Imager and Slitless Spectrograph (NIRISS; [Doyon et al. 2012](#)). Since MIRI imaging has a very large point-spread-function (PSF) ($> 1''$ for wavelengths $> 7.5 \mu\text{m}$) compared to NIRCam, we do not consider mid-infrared data in this work. Moreover, slitless spectroscopy is subject to strong spectral contamination, especially in crowded fields like the core of SMACS J0723. We have checked the NIRSpec targets available in the Mikulski Archive for Space Telescopes (MAST³) portal. Only one is a multiple image family, images 4b and 4c. Unfortunately, the spectra available at MAST do not show any clear spectral feature that could be used to measure its redshift. Therefore, we focus our work only on NIRCam imaging to identify new multiple image families not detected with *HST*.

3.1. NIRCam data reduction

NIRCam ERO observations of SMACS J0723 were carried out in the filters F090W, F150W, F200W, F277W, F356W and F444W, covering the wavelength range from 0.8 μm to $\approx 5.0 \mu\text{m}$, under the programme ID 2736 (P.I.: K. Pontoppidan). The total exposure time in each filter was 7537 seconds divided over nine dither patterns, ensuring enough depth to detect and resolve faint sources. We use the standard NIRCam reduction pipeline with the calibration filter available with the first data release. We produced mosaics with resolution of 20mas/pixel for the F090W, F150W and F200W filters, and 40mas/pixel for F277W, F356W and F444W.

The final mosaics cover the core of SMACS J0723 and the entire region of multiple image formation. In Figure 1, we show the color composite image created using the software *trilogy*

² <http://archive.eso.org/cms.html>

³ <https://mast.stsci.edu/portal/>

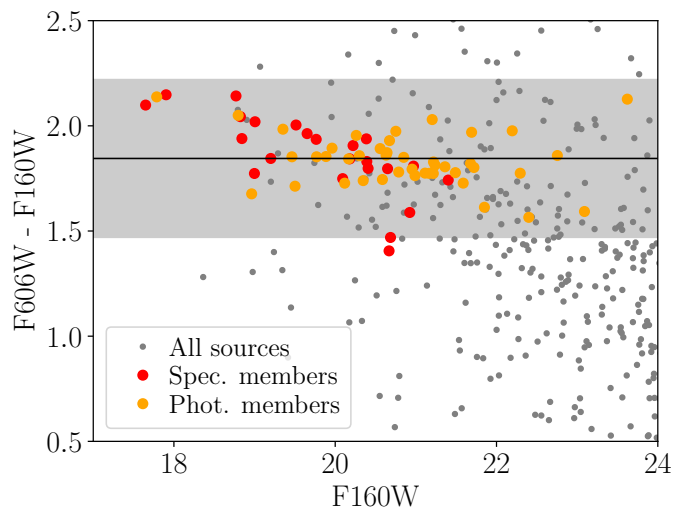


Fig. 2. Color magnitude diagram of galaxies in the field of view of SMACS J0723. The spectroscopically confirmed cluster members (red points) define the red sequence (grey band) that is used to select photometrically 38 additional cluster members (orange points) down to magnitude of 24 in F160W.

(Coe et al. 2012). We aligned the final images to the RELICS *HST* data to maintain the same coordinate reference with previous observations. This introduces a small rigid offset with respect to the nominal coordinates of ERO release. The astrometric precision between *JWST* and *HST* data we obtained has an r.m.s. of $0''.015$. Moreover, because of the nature of these *JWST* early observations, the calibration files are not ideal and the absolute flux calibration might have some issues. Nonetheless, these caveats do not influence the colors and morphology of multiple images in the imaging, and have no significant effect on our lens model.

4. Strong lens model

We used the software `lenstool` (Kneib et al. 1996; Jullo et al. 2007; Jullo & Kneib 2009) to model the mass distribution of SMACS J0723. The fiducial mass model consists of an elliptical cluster-scale dark matter halo (6 free parameters), a truncated spherical isothermal mass profile for each cluster galaxy member (2 free parameters with constant M/L scaling relation for the members), and an external shear (2 free parameters). The model constraints are the positions of multiple images and (when available) spectroscopic redshifts. For families of multiple images with no spectroscopic measurements, we allow the redshift values free to vary in the model. We built two versions of the lens model, one using information from *HST* and MUSE only, i.e. prior to the *JWST* ERO release. The second model was built upon *JWST* NIRC*am* imaging, which allowed us to confirm 27 additional, secure multiple images from 10 individual sources. Naturally, these new identifications are extremely faint or not detected in the *HST* optical and near-IR imaging. We checked carefully the MUSE data-cube around these positions, but as expected, no optical emission was detected. In the following sections, we describe the two models we present in this work.

4.1. Pre-*JWST* lens model

Before the release of *JWST*/NIRC*am* imaging, the best data set available on SMACS J0723 was photometry from the RELICS

program and spectroscopy from MUSE (see Sections 2.1 and 2.2). From the spectroscopic data, we confirm a total of 23 cluster members in the redshift range of $0.367 - 0.408$, corresponding to a rest-frame velocity of ± 3000 km/s from the cluster mean redshift of $z=0.387$. However, the spectroscopic confirmed members are limited to the MUSE field of view of 1 arcmin^2 . We use the color and photometric redshift information of confirmed members to expand the member selection to the outer regions of the cluster. In Figure 2, we show the color-magnitude diagram for the *HST* filters F606W and F160W, where the red sequence is clearly defined by the spectroscopically confirmed members. In total, we selected 38 photometric members down to a magnitude of 24 in F160W.

From the MUSE spectroscopy, we confirmed the redshifts of 4 families of multiple images. In Table 1, we list all the positions and redshifts of multiple images used as constraints in the lens model. In this first version of the model, two families have no secure spectroscopic confirmations, but are clearly detected in *HST* and have colors and parities as expected in strong lensing. Our pre-*JWST* model thus has 19 multiple images as input from 6 families, of which only two of the redshifts are free to vary in the model.

The mass profiles we adopted are the pseudo-isothermal elliptical parameterization (PIEMD, Kassiola & Kovner 1993) to describe the extended cluster mass (dark matter), and dual pseudo isothermal mass profile with axial symmetry (Elíasdóttir et al. 2007; Suyu & Halkola 2010) to describe the 61 cluster members. As commonly done in the literature, we assume a constant mass-to-light ratio for the cluster members. With this, the number of free parameters describing these components are reduced to two normalizations, namely $\sigma_{v,\text{gals}}^{\text{norm.}}$ and $r_{\text{cut,gals}}^{\text{norm.}}$. Finally, we have also considered an external shear component to account for external massive perturbers that can affect the light deflection of background sources.

Our fiducial cluster mass model was obtained following the procedure in Caminha et al. (2019), in order to find the combination of mass profiles that can reproduce well the position of multiple images while not overfitting the data. We tested a range of combinations of mass profiles, from the most simple one composed by a single PIEMD halo profile plus cluster members, to models with additional cluster halo components, external shear, and individual cluster members with mass parameters varying freely outside the mass-to-light scaling relation. We found that the parameterization with the smallest values of the Bayesian information criterion (BIC, Schwarz 1978) and Akaike information criterion (AICc, Akaike 1974), is the one with ten parameters for the mass distribution (as described at the beginning of Section 4) and the two unknown redshifts of families 1 and 4 (see Table 1). In this model, the best-fit offset between the observed multiple images and the model predicted positions is $\delta_{\text{rms}} = 0''.39$. We note that our best-fit δ_{rms} is significantly lower than previously obtained by Golubchik et al. (2022), who quoted a value of $\delta_{\text{rms}} = 2''.3$.

4.2. *JWST* lens model

With the new *JWST*/NIRC*am* imaging, at wavelengths not reachable with *HST* and the high spatial resolution, we were able to improve significantly our lens model constraints. We have carefully inspected the near-IR imaging in order to find new multiple images that were not previously identified. Thanks to the color information and resolution, we obtain a sample of 27 new secure multiple images from ten background galaxies, increasing

by a factor of two the number of model constraints compared to the pre-*JWST* (*HST* and MUSE only) lens model.

Given that these sources are very faint in observed optical wavelengths, none have spectroscopic confirmation from MUSE, and in most cases, they have no clear *HST* counterpart. In Table 1, we list all new multiple images as well as their model redshifts. Moreover, in Figure A.2, we show the *JWST* NIRCcam cut-outs around all multiple images used in our lens model.

The lens model with the new multiple images has a best-fit δ_{rms} of 0′.51. Considering that the number of model constraints is around twice than that of the pre-*JWST* model, this small increase on δ_{rms} is expected. Nonetheless, it is significantly lower than previous published works on SMACS J0723. In Figure 1, we show the critical line for a source at $z = 10$ overlaid on the *JWST*/NIRCcam imaging. The lens model, including magnification maps and `lenstool` configuration files are available in the electronic version of this manuscript and upon request to the authors. We encourage the community to further explore the lens model presented in this work.

In Table A.2 we list the constrained total mass parameters and in Figure A.1 we show the total mass and density profiles. We find a mass of $8.6^{+0.2}_{-0.2} \times 10^{13} M_{\odot}$ at a radius of 128 kpc, approximately the Einstein radius for a source at $z \rightarrow \infty$. At this radius, this mass estimate is 33% more accurate when comparing to our pre-*JWST* lens model.

One special case is family 7. Images 7a and 7b are secure multiple images because of their colors and morphology shown in Figure A.2. They are composed by two main clumps, and some smaller possible substructures. Image #7c is a very likely counter-image showing similar colour and the double clump morphology. In order to avoid any bias in our lens model, we do not include #7c as an observational constraint. The total lensing magnifications are $6.0^{+0.8}_{-0.7}$, $9.8^{+0.9}_{-1.1}$, and $4.5^{+0.5}_{-0.5}$ for 7a, 7b and #7c, respectively. The multiple images are located in the easternmost region of the cluster (see Figure 1). This makes it difficult to precisely constraint its redshift from the model. However, the lens model indicates it might be at $z > 7.5$ from the posterior probability distribution.

4.3. Comparison to models in the literature

Mahler et al. (2022) and Pascale et al. (2022) have also used the new *JWST* observations, particularly the imaging, to model SMACS J0723. The model by Pascale et al. (2022) was built upon the model of Golubchik et al. (2022) based on *HST* observations, before the *JWST* ERO. We briefly compare our model ingredients and results to these studies.

All studies identified new families of multiple images in the NIRCcam imaging: 16 in Mahler et al. (2022), 13 in Pascale et al. (2022) and 10 in this work. Since all families have no spectroscopic redshift confirmations (except one identified by Mahler et al. (2022) with NIRSpc), we have deliberately used only highly secure families of multiple image (in Table 1) to constrain our mass model, in order to avoid misidentifications of families that could bias our mass model parameters. This explains our lower number of families reported.

All three models are parametric in having a cluster halo component with cluster members, and we have a further external shear component that is not present in the other two studies. Our robust selection of 61 cluster members is based on both MUSE spectroscopy and *HST* photometry, whereas Mahler et al. (2022) used only MUSE to identify 26 members and Pascale et al. (2022) relied on *HST* photometry to identify ~ 133 members (that will be refined in future work by including spectroscopy).

Pascale et al. (2022) have measured photometric redshifts based on the NIRCcam photometry and also predicted the redshifts based on their mass model. Both Pascale et al. (2022) and our model produced 10 redshift estimates for the new *JWST* lensed sources, although only 6 of the 10 are in common. While the model redshifts from both models for 5 of these sources are all in the range $\sim 1 - 3$, only 1 of the 5 agrees within the 1σ uncertainty. The 6th source is our family 7 at $z > 7.5$, whereas its redshift is unconstrained by Pascale et al. (2022). The model redshifts are therefore highly model dependent, and relies on the goodness of the model fits. Future spectroscopic redshift measurements of some of these sources would be valuable.

Even though a direct comparison of the different models is not straightforward given the different families of multiple images used, the δ_{rms} of the models provides an indication of the goodness of the model fit. Our δ_{rms} of 0′.51 is a factor of ~ 2 lower than the 1′.08 from Mahler et al. (2022) and 0′.93 from Pascale et al. (2022). We attribute our better fitting model to (1) our use of only the secure families of multiple images, and (2) our robust cluster member selection based on both spectroscopy and photometry.

5. Conclusions

We present our strong lens model of SMACS J0723, the first gravitational lens ever observed by *JWST*, using newly available data from NIRCcam. With the new data, we doubled the number of model constraints, increasing the number of multiple images from 19 identified with *HST* and MUSE data, to 47. This demonstrates the unique capabilities of *JWST* in discovering faint and/or high-redshift galaxies that were previously undetected in *HST* observations. Our lens model is capable of reproducing the positions of all multiple images with a high accuracy of $\delta_{\text{rms}} = 0′.51$. We report the lens model redshifts for 12 lensed galaxies, most of them very faint and remain challenging to obtain spectroscopic information. While most of the lensed galaxies have modeled redshifts $\lesssim 3$, one object stands out as a high-redshift galaxy at $z > 7.5$ with image 7b having a magnification of $|\mu| \approx 9.8^{+0.9}_{-1.1}$. This might be the first galaxy with spatially resolved substructures at the epoch of re-ionization of the Universe (see Figure A.2), and an interesting target for follow-up deep spectroscopy. We report spectroscopic redshifts from MUSE archival data and their lensing magnifications. Finally, our lens models, including magnification maps, configuration files for the software `lenstool` are made publicly available.

These first observations by *JWST* of SMACS J0723 have proven to be a treasure trove, allowing us to reduce the uncertainties in our cluster mass measurements by 33% even without incorporating any spectroscopic information on the newly identified lensed galaxies. We anticipate future *JWST* observations of other strong lensing galaxy clusters to be transformative in both constraining cluster mass distributions and studying high-redshift galaxies.

Acknowledgements. We thank C. Grillo, P. Rosati and D. Sluse for constructive discussions during the preparation of this work. GBC and SHS acknowledge the Max Planck Society for financial support through the Max Planck Research Group for SHS and the academic support from the German Centre for Cosmological Lensing. AM, PB, AA and EV acknowledge financial contributions by PRIN-MIUR 2017WSCC32 “Zooming into dark matter and proto-galaxies with massive lensing clusters” (P.I.: P.Rosati), INAF “main-stream” 1.05.01.86.20: “Deep and wide view of galaxy clusters” (P.I.: M. Nonino) and INAF “main-stream” 1.05.01.86.31 “The deepest view of high-redshift galaxies and globular cluster precursors in the early Universe” (P.I.: E. Vanzella). AA has received funding from the European Union’s Horizon 2020 research and innovation programme under the Marie Skłodowska-Curie grant agreement No 101024195 - ROSEAU.

References

- Acebron, A., Jullo, E., Limousin, M., et al. 2017, *MNRAS*, 470, 1809
- Akaike, H. 1974, *IEEE Transactions on Automatic Control*, 19, 716
- Atek, H., Richard, J., Kneib, J.-P., et al. 2015, *ApJ*, 800, 18
- Bouchet, P., García-Marín, M., Lagage, P. O., et al. 2015, *PASP*, 127, 612
- Bradač, M., Clowe, D., Gonzalez, A. H., et al. 2006, *ApJ*, 652, 937
- Caminha, G. B., Grillo, C., Rosati, P., et al. 2016a, *A&A*, 587, A80
- Caminha, G. B., Grillo, C., Rosati, P., et al. 2017a, *A&A*, 600, A90
- Caminha, G. B., Grillo, C., Rosati, P., et al. 2017b, *A&A*, 607, A93
- Caminha, G. B., Karman, W., Rosati, P., et al. 2016b, *A&A*, 595, A100
- Caminha, G. B., Rosati, P., Grillo, C., et al. 2019, *A&A*, 632, A36
- Caminha, G. B., Suyu, S. H., Grillo, C., & Rosati, P. 2022, *A&A*, 657, A83
- Clowe, D., Bradač, M., Gonzalez, A. H., et al. 2006, *ApJ*, 648, L109
- Coe, D., Salmon, B., Bradač, M., et al. 2019, *ApJ*, 884, 85
- Coe, D., Umetsu, K., Zitrin, A., et al. 2012, *ApJ*, 757, 22
- Doyon, R., Hutchings, J. B., Beaulieu, M., et al. 2012, in *Society of Photo-Optical Instrumentation Engineers (SPIE) Conference Series*, Vol. 8442, *Space Telescopes and Instrumentation 2012: Optical, Infrared, and Millimeter Wave*, ed. M. C. Clampin, G. G. Fazio, H. A. MacEwen, & J. Oschmann, Jacobus M., 84422R
- Ebeling, H., Edge, A. C., & Henry, J. P. 2001, *ApJ*, 553, 668
- Elíasdóttir, Á., Limousin, M., Richard, J., et al. 2007, *arXiv e-prints*, arXiv:0710.5636
- Golubchik, M., Furtak, L. J., Meena, A. K., & Zitrin, A. 2022, *arXiv e-prints*, arXiv:2207.05007
- Grillo, C., Rosati, P., Suyu, S. H., et al. 2018, *ApJ*, 860, 94
- Grillo, C., Rosati, P., Suyu, S. H., et al. 2020, *ApJ*, 898, 87
- Jakobsen, P., Ferruit, P., Alves de Oliveira, C., et al. 2022, *A&A*, 661, A80
- Jullo, E. & Kneib, J. P. 2009, *MNRAS*, 395, 1319
- Jullo, E., Kneib, J. P., Limousin, M., et al. 2007, *New Journal of Physics*, 9, 447
- Jullo, E., Natarajan, P., Kneib, J. P., et al. 2010, *Science*, 329, 924
- Kassiola, A. & Kovner, I. 1993, *ApJ*, 417, 450
- Kelly, P. L., Rodney, S. A., Treu, T., et al. 2015, *Science*, 347, 1123
- Kneib, J. P., Ellis, R. S., Smail, I., Couch, W. J., & Sharples, R. M. 1996, *ApJ*, 471, 643
- Mahler, G., Jauzac, M., Richard, J., et al. 2022, *arXiv e-prints*, arXiv:2207.07101
- Pascale, M., Frye, B., Diego, J., et al. 2022, *arXiv e-prints*, arXiv:2207.07102
- Refsdal, S. 1964, *MNRAS*, 128, 307
- Repp, A. & Ebeling, H. 2018, *MNRAS*, 479, 844
- Rieke, G. H., Wright, G. S., Böker, T., et al. 2015, *PASP*, 127, 584
- Rieke, M. J., Kelly, D., & Horner, S. 2005, in *Society of Photo-Optical Instrumentation Engineers (SPIE) Conference Series*, Vol. 5904, *Cryogenic Optical Systems and Instruments XI*, ed. J. B. Heaney & L. G. Burriesci, 1–8
- Rigby, J., Perrin, M., McElwain, M., et al. 2022, *arXiv e-prints*, arXiv:2207.05632
- Schwarz, G. 1978, *Ann. Statist.*, 6, 461
- Soto, K. T., Lilly, S. J., Bacon, R., Richard, J., & Conseil, S. 2016, *MNRAS*, 458, 3210
- Suyu, S. H. & Halkola, A. 2010, *A&A*, 524, A94
- Suyu, S. H., Marshall, P. J., Auger, M. W., et al. 2010, *ApJ*, 711, 201
- Vanzella, E., Caminha, G. B., Rosati, P., et al. 2021, *A&A*, 646, A57
- Vanzella, E., Meneghetti, M., Caminha, G. B., et al. 2020, *MNRAS*, 494, L81
- Weillbacher, P. M., Palsa, R., Streicher, O., et al. 2020, *A&A*, 641, A28

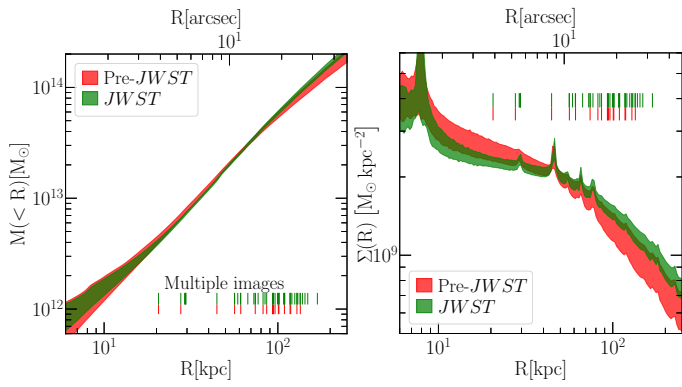


Fig. A.1. Total mass and density profiles of SMACS J0723 from our pre-*JWST* (red) and *JWST* (green) lens models. The regions correspond to the 95% confidence, and the positions of multiple images are indicated by vertical lines.

Appendix A: Supporting material

In this appendix, we present the supporting material of this work. The full redshift catalogue from the MUSE data and the lensing magnification estimates from the *JWST* model are presented in Table A.1. In Table A.2, we show the recovered mass model parameters for the *JWST* lens model, and the total mass and density profiles in Figure A.1. Figure A.2 shows the cut-outs of all multiple images used in our lens models, and Figure A.3, the spectra of confirmed multiple images.

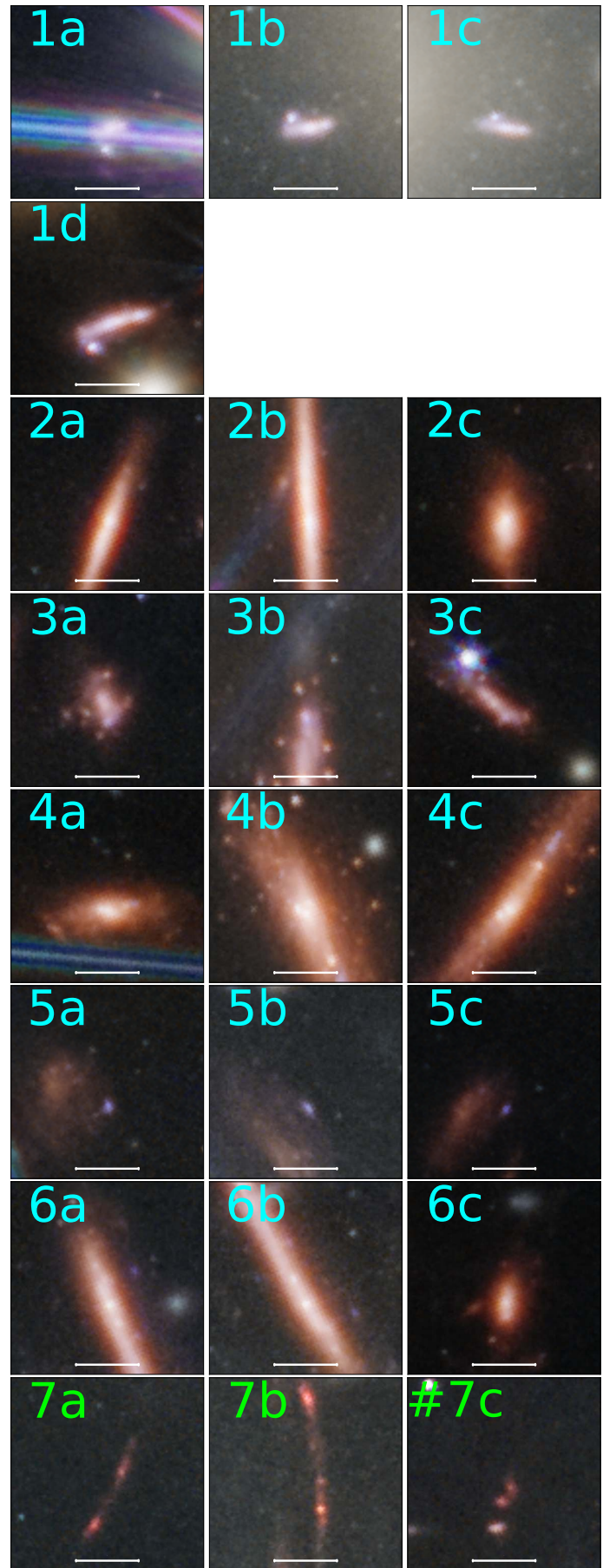


Fig. A.2. Multiple image cut-outs. The white scale bar has 1'' length.

Table A.1. MUSE spectroscopic catalogue.

ID	RA	Dec	z_{MUSE}	QF	mult.	$ \mu $	$\delta \mu $ min	$\delta \mu $ max
1	110.8284294	-73.4602574	0.0000	4	1	1.000	0.000	0.000
2	110.8479302	-73.4616212	0.0000	4	1	1.000	0.000	0.000
3	110.8334991	-73.4484003	0.0000	4	1	1.000	0.000	0.000
4	110.8080566	-73.4466289	0.0000	4	1	1.000	0.000	0.000
5	110.8075712	-73.4469594	0.0000	4	1	1.000	0.000	0.000
6	110.8261351	-73.4486167	0.0000	4	1	1.000	0.000	0.000
7	110.8235839	-73.4499063	0.0000	4	1	1.000	0.000	0.000
8	110.8235958	-73.4474173	0.0000	4	1	1.000	0.000	0.000
9	110.8066750	-73.4516338	0.0000	4	1	1.000	0.000	0.000
10	110.8117026	-73.4532181	0.0000	4	1	1.000	0.000	0.000
11	110.8354266	-73.4530012	0.0000	4	1	1.000	0.000	0.000
12	110.8404555	-73.4533044	0.0000	4	1	1.000	0.000	0.000
13	110.8166004	-73.4551109	0.0000	4	1	1.000	0.000	0.000
14	110.8450243	-73.4553745	0.0000	4	1	1.000	0.000	0.000
15	110.8354564	-73.4557020	0.0000	4	1	1.000	0.000	0.000
16	110.8178433	-73.4544317	0.0000	4	1	1.000	0.000	0.000
17	110.8040760	-73.4581786	0.0000	4	1	1.000	0.000	0.000
18	110.8230292	-73.4593733	0.0000	4	1	1.000	0.000	0.000
19	110.8367020	-73.4585449	0.0000	4	1	1.000	0.000	0.000
20	110.8486872	-73.4593321	0.0000	4	1	1.000	0.000	0.000
21	110.8495683	-73.4625124	0.3217	3	1	1.000	0.000	0.000
22	110.8362871	-73.4568771	0.3241	3	1	1.000	0.000	0.000
23	110.8252476	-73.4545586	0.3774	3	1	1.000	0.000	0.000
24	110.8243781	-73.4599050	0.3806	3	1	1.000	0.000	0.000
25	110.8557313	-73.4557427	0.3822	3	1	1.000	0.000	0.000
26	110.8530957	-73.4566588	0.3836	3	1	1.000	0.000	0.000
27	110.8161206	-73.4511937	0.3844	3	1	1.000	0.000	0.000
28	110.8456507	-73.4513365	0.3847	3	1	1.000	0.000	0.000
29	110.8538419	-73.4500630	0.3848	3	1	1.000	0.000	0.000
30	110.8185163	-73.4552171	0.3849	3	1	1.000	0.000	0.000
31	110.8045012	-73.4561504	0.3864	3	1	1.000	0.000	0.000
32	110.8550113	-73.4501908	0.3865	3	1	1.000	0.000	0.000
33	110.8377986	-73.4536001	0.3865	3	1	1.000	0.000	0.000
34	110.8326866	-73.4569116	0.3869	3	1	1.000	0.000	0.000
35	110.8562438	-73.4506971	0.3872	2	1	1.000	0.000	0.000
36	110.8257093	-73.4586938	0.3888	3	1	1.000	0.000	0.000
37	110.8376015	-73.4561834	0.3896	3	1	1.000	0.000	0.000
38	110.8024677	-73.4586733	0.3905	3	1	1.000	0.000	0.000
39	110.8182380	-73.4546131	0.3909	3	1	1.000	0.000	0.000
40	110.8401314	-73.4558252	0.3911	3	1	1.000	0.000	0.000
41	110.8268052	-73.4546385	0.3914	3	1	1.000	0.000	0.000
42	110.8264520	-73.4549705	0.3915	3	1	1.000	0.000	0.000
43	110.8184078	-73.4482682	0.3932	2	1	1.000	0.000	0.000
44	110.8006165	-73.4485206	0.3940	3	1	1.000	0.000	0.000
45	110.8487541	-73.4603147	0.3970	3	1	1.000	0.000	0.000
46	110.8368347	-73.4565146	0.3980	3	1	1.000	0.000	0.000
47	110.8049026	-73.4494579	0.4138	2	1	1.093	-0.003	+0.004
48	110.8418679	-73.4567000	0.4233	3	1	1.190	-0.005	+0.005
49	110.8521136	-73.4555097	0.5189	3	1	1.654	-0.025	+0.017
50	110.8327947	-73.4466290	0.6002	3	1	1.524	-0.043	+0.038
51	110.8302846	-73.4604916	0.7455	3	1	2.139	-0.101	+0.094
52	110.8089116	-73.4609025	0.7460	3	1	1.921	-0.077	+0.067
53	110.8384789	-73.4492352	0.7469	3	1	2.304	-0.117	+0.103
54	110.8035266	-73.4573758	0.9366	3	1	3.699	-0.165	+0.166
55	110.8523022	-73.4594938	1.0815	3	1	3.030	-0.163	+0.149
56	110.8533363	-73.4595550	1.0815	3	1	3.107	-0.170	+0.159
57	110.8535225	-73.4591817	1.0823	3	1	3.205	-0.173	+0.157
58	110.8101344	-73.4605069	1.0826	3	1	2.706	-0.171	+0.163
59	110.8566353	-73.4587921	1.0833	3	1	3.239	-0.161	+0.154
60	110.8557579	-73.4588674	1.0833	3	1	3.220	-0.153	+0.150
61	110.8066813	-73.4523137	1.2696	9	1	17.552	-2.160	+2.449
62	110.8363455	-73.4587211	1.3782	3	3	60.529	-20.060	+66.252
63	110.8385802	-73.4509557	1.3782	3	3	8.727	-1.106	+1.158
64	110.8405311	-73.4551527	1.3782	3	3	6.269	-0.721	+0.777
65	110.8156178	-73.4602436	1.3802	9	1	3.515	-0.296	+0.302
66	110.8207008	-73.4506760	1.3825	9	3	5.203	-0.544	+0.562
67	110.8162336	-73.4534926	1.3825	9	3	12.862	-1.920	+1.753
68	110.8171040	-73.4589089	1.3825	9	3	9.072	-1.262	+1.278
69	110.8222252	-73.4526676	1.4254	3	1	30.882	-6.622	+8.110
70	110.8236935	-73.4518167	1.4254	3	2	47.895	-6.497	+8.323
71	110.8405974	-73.4510474	1.4503	3	3	6.709	-0.793	+0.844
72	110.8427896	-73.4546490	1.4503	3	3	23.382	-4.246	+5.161
73	110.8388169	-73.4587230	1.4503	3	3	10.237	-1.396	+1.476
74	110.8485993	-73.4606870	1.4792	9	1	3.400	-0.252	+0.241
75	110.8520623	-73.4525378	1.4816	3	1	10.197	-0.880	+0.886
76	110.8519575	-73.4523356	1.4817	3	1	9.487	-0.811	+0.849
77	110.8053717	-73.4499939	3.3136	9	1	91.691	-46.910	+229.211
78	110.7998624	-73.4549695	3.4287	9	1	17.777	-3.177	+3.711

Notes. Spectroscopic confirmations from MUSE. The columns QF is the quality flag of the MUSE confirmation, where 3 corresponds to a secure measurement, 2 to a probable secure redshift, 9 to a measurement based on a single emission line, and 4 to a secure star confirmation. Multiple images are indicated in the mult. column, and magnification factors with the error bars are also indicated in columns μ and δ_m min/max (68% confidence interval).

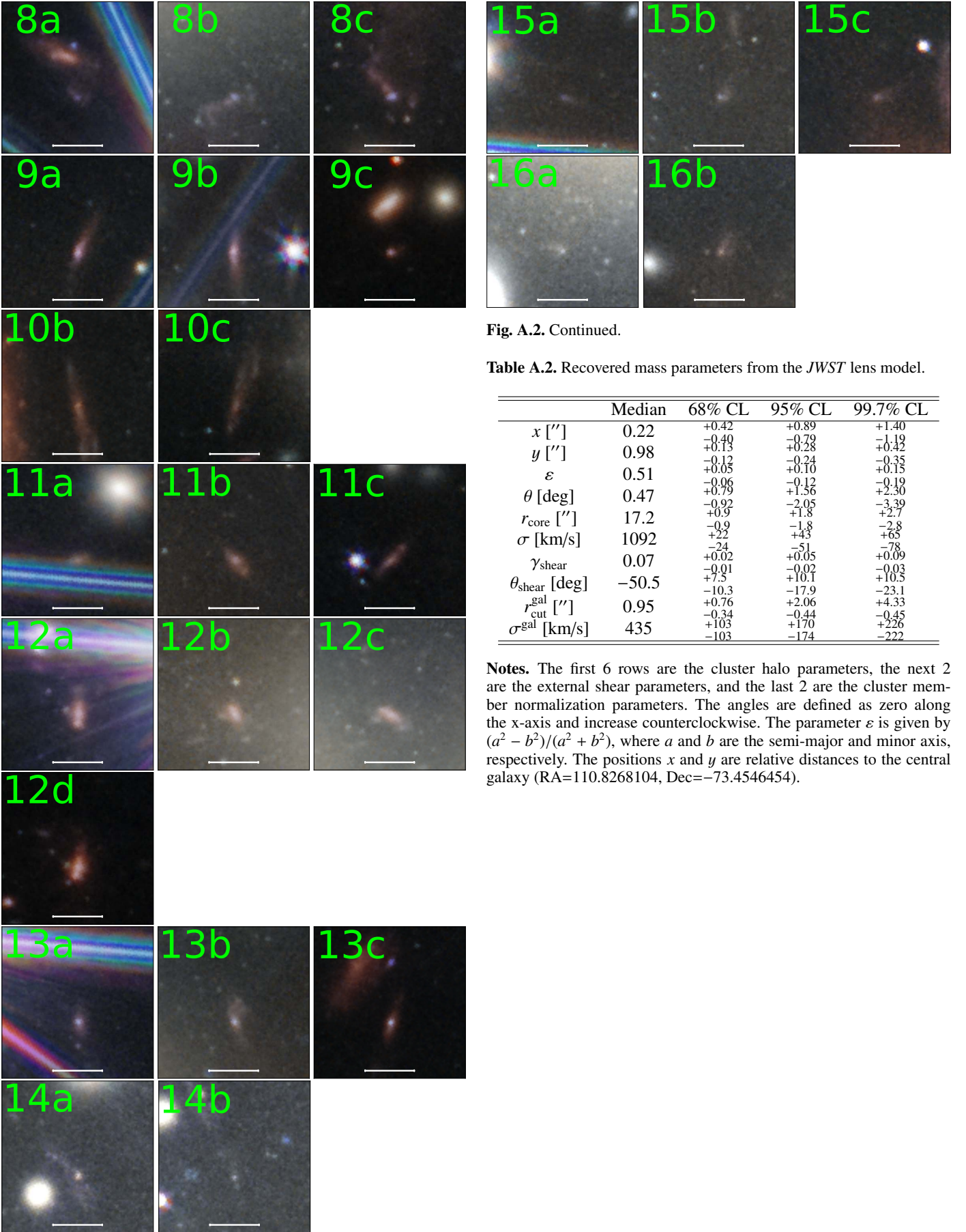


Fig. A.2. Continued.

 Table A.2. Recovered mass parameters from the *JWST* lens model.

	Median	68% CL	95% CL	99.7% CL
x ["]	0.22	+0.42	+0.89	+1.40
y ["]	0.98	-0.40	-0.79	-1.19
ε	0.51	+0.13	+0.28	+0.42
θ [deg]	0.47	-0.12	-0.24	-0.35
r_{core} ["]	17.2	+0.05	+0.10	+0.15
σ [km/s]	1092	-0.06	-0.12	-0.19
γ_{shear}	0.07	+0.79	+1.56	+2.30
θ_{shear} [deg]	-50.5	-0.92	-2.05	-3.39
$r_{\text{cut}}^{\text{gal}}$ ["]	0.95	+0.9	+1.8	+2.7
σ^{gal} [km/s]	435	-24	-51	-78
		+22	+43	+65
		+0.02	+0.05	+0.09
		-0.01	-0.02	-0.03
		+7.5	+10.1	+10.5
		-10.3	-17.9	-23.1
		+0.76	+2.06	+4.33
		-0.34	-0.44	-0.45
		+103	+170	+226
		-103	-174	-222

Notes. The first 6 rows are the cluster halo parameters, the next 2 are the external shear parameters, and the last 2 are the cluster member normalization parameters. The angles are defined as zero along the x-axis and increase counterclockwise. The parameter ε is given by $(a^2 - b^2)/(a^2 + b^2)$, where a and b are the semi-major and minor axis, respectively. The positions x and y are relative distances to the central galaxy (RA=110.8268104, Dec=-73.4546454).

Fig. A.2. Continued.

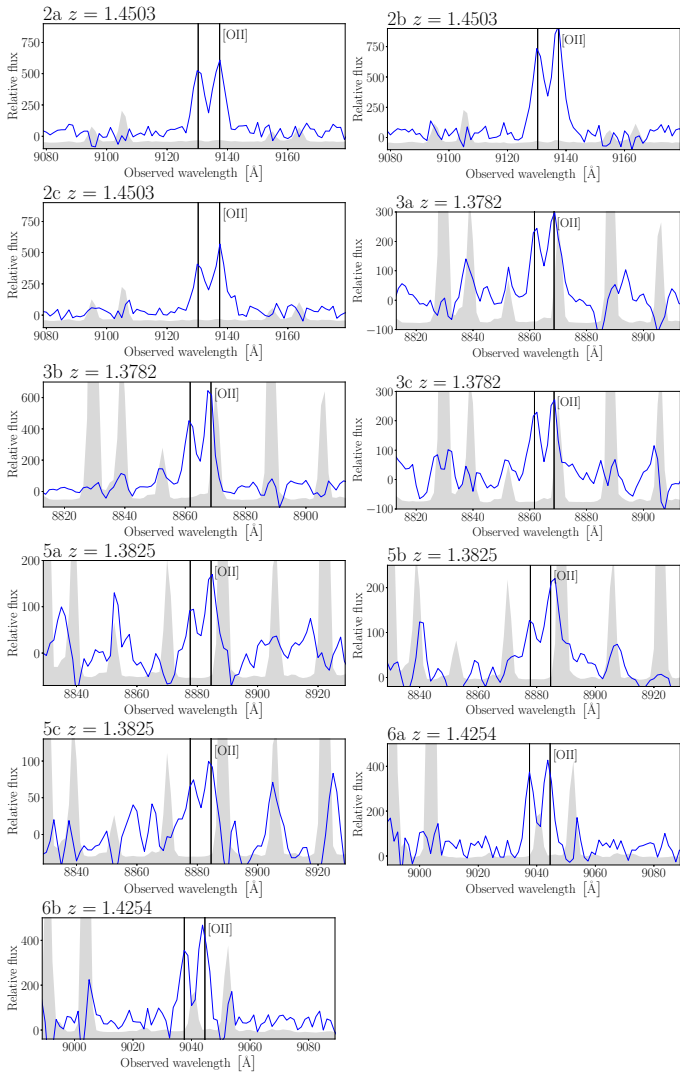


Fig. A.3. MUSE spectrum of confirmed multiple images. Blues lines are the spectrum extracted from the data cube, and the shaded regions are the re-scaled variance. Vertical lines indicate the O II emission at the source redshift.